Visual Neuroscience (2001), **18**, 835–848. Printed in the USA.

DOI: 10.1017.S0952523801155161

Asymmetrical dynamics of voltage spread in retinal horizontal cell networks

J. BENDA,[1] R. BOCK,[2] P. RUJAN,[3] AND J. AMMERMÜLLER[2]

[1]Innovationskolleg Theoretische Biologie, Humboldt-Universität Berlin, Germany
[2]Fachbereich Biologie, Carl von Ossietzky Universität, Oldenburg, Germany
[3]Fachbereich Physik, Carl von Ossietzky Universität, Oldenburg, Germany

(RECEIVED September 27, 2000; ACCEPTED August 24, 2001)

Abstract

Lateral voltage spread in electrically coupled retinal horizontal cell networks is the substrate of center-surround antagonism in bipolar and ganglion cells. We studied its spatial and temporal properties in more detail in turtle L1 horizontal cells by using a contrast border as light stimulus. Experimental data were contrasted with expectations from a linear continuum model to specify the impact of nonlinearities. The assumptions for the diffusion term of the continuum model were justified by neurobiotin labeling. Measured voltage spread revealed two different length constants Λ_+ and Λ_0, under illuminated and nonilluminated regions of the retina, respectively, as predicted by the linear model. Length constants in the illuminated region showed strong temporal dynamics. For the initial phase of the horizontal cell responses Λ_+ was larger than Λ_o. This was also in accordance with the model. Right at the peak of the response, however, Λ_+ dropped below Λ_o and did not change any more. It is this temporal reversal of asymmetry in voltage spread and not the decrease of Λ_+ itself that is lacked by the linear model. The observed independence of the mean ratio Λ_+/Λ_o from light intensity in both the peak and the plateau phases of horizontal cell responses contradicts the linear assumption, too. These two effects have to be addressed to local nonlinearities in the horizontal cell network like a negative feedback loop from photoreceptors and/or voltage-dependent conductances. Due to the failure of the linear model, firm conclusions about the membrane resistance and the coupling resistance of the horizontal cell network cannot be drawn from length constant measurements.

Keywords: Turtle retina, Gap junctions, Electrical coupling, Continuum model, Length constant

Introduction

Electrical coupling of retinal horizontal cells through gap junctions has been confirmed by many studies (Tomita, 1957; Boroviagin, 1966; Naka & Rushton, 1967; Raviola, 1976; Norton et al., 1968; Kaneko, 1971). It allows for voltage spread over several millimeters across the retina, playing a major role in the genesis of center-surround antagonism of bipolar and ganglion cell receptive fields (Naka & Witkovsky, 1972; Werblin, 1974; Thibos & Werblin, 1978; Mangel, 1991) and in gain control of photoreceptor synapses (Wu, 1992, 1994; Burkhardt, 1993; Piccolino, 1995). In the turtle retina all horizontal cell types are homologically coupled, constituting separate conducting networks (Byzov, 1975; Gerschenfeld et al., 1982; Piccolino, 1995; Ammermüller & Kolb, 1996). Since the coupling is nonrectifying (Kaneko, 1971; DeVries & Schwartz, 1989) and voltage spreads over several cells, these networks can be considered as a continuum and the lateral network currents can be modeled by a simple diffusion equation (Naka & Rushton, 1967; Lamb, 1976).

Besides the diffusion through the syncytium, voltage spread is also influenced by the membrane conductances of the horizontal cells. These include nonlinear voltage-gated channels (Byzov & Trifonov, 1981; Winslow & Knapp, 1991; Akopian et al., 1997) and postsynaptic channels, driven by photoreceptors, which again may be modulated by feedback mechanisms from the horizontal cells (Wu, 1992; Burkhardt, 1993; Piccolino, 1995; Verweij et al., 1996*a*; Kamermans & Spekreijse, 1999; Kamermans et al., 2001).

The linear continuum model introduced by Naka and Rushton (1967) and simplified by Lamb (1976) does not consider any of the possible nonlinear mechanisms. However, it has long been used for analysis of voltage spread in horizontal cells (Lamb & Simon, 1976; Owen & Hare, 1989; Lankheet et al., 1990; Andreu et al., 2000). The model connects the microscopic properties membrane resistance r_m and sheet resistance R_s of the syncytium directly with the characteristic length of the macroscopically observed exponential voltage decay—the length constant λ. Provided the assumption of a linear membrane is valid, it is possible to gain some information about r_m and R_s by means of λ. Two methods for determining λ were introduced in the past: light bars moved across the

Address correspondence and reprint requests to: J. Ammermüller, Department of Biology, Postfach 2503, Carl von Ossietzky University, Oldenburg, D-26111 Oldenburg, Germany. E-mail: josef.ammermueller@uni-oldenburg.de

retina and spots of increasing diameter (Byzov & Shura-Bura, 1983; Piccolino et al., 1984; Lankheet et al., 1990; Perlman & Ammermüller, 1994). Both methods assume a constant membrane resistance, implying that neither the stimulating light or feedback mechanisms have an effect on λ. This simple model, however, failed to explain experimental data (Marmarelis & Naka, 1972; Yagi & Kaneko, 1987; Lankheet et al., 1993; Kamermans et al., 1996; Umino & Ushio, 1998). The measured length constant is dynamic during the response time of the horizontal cells and depends on intensity in several species (Lamb, 1976; Byzov & Shura-Bura, 1983; Perlman & Ammermüller, 1994; Reifsnider & Tranchina, 1995; Ammermüller et al., 1996; Verweij et al., 1996*b*; Kamermans et al., 1996; Umino & Ushio, 1998). Compartmental modeling, taking time- and voltage-dependent conductances into account, predicted an increase of λ with time and increasing background illumination (Winslow & Knapp, 1991). Such compartmental models, on the other hand, still contain a large number of quantitatively unknown, free parameters, which makes interpretation very difficult.

In this study, we derived the continuum model in more detail to work out all the involved assumptions. The geometrical conditions of the continuum approximation were examined by neurobiotin labeling of the horizontal cell network. We extended the linear continuum model to the general case where the length constant depends on the photoreceptors' activity *via* the membrane resistance r_m of the horizontal cells. In this case, the length constants observed in dark regions should be smaller than those in illuminated regions of the retina. This expectation was tested by directly measuring voltage spread in illuminated and nonilluminated parts of the horizontal cell syncytium. By this way, we determined precisely to what extent the linear model is capable to explain the experimental data, and where nonlinear effects have to be taken into account.

Methods

Model

In the continuum limit, the membrane potential V in horizontal cell networks can be modeled by a diffusion-like two-dimensional partial differential equation—the plate equation—with global parameters τ (time constant), λ (length constant), and E (full-field potential):

$$\tau \partial V/\partial t = \lambda^2 \Delta V - V + E, \tag{1}$$

where Δ is the Laplacian, the second-order spatial derivative (Naka & Rushton, 1967; Lamb, 1976; Lamb & Simon, 1976). A detailed derivation of the plate eqn. (1) is provided in the Appendix. The total membrane resistance r_m per unit area of the sheet (not the membrane of the cells!) is given by $1/r_m = \sum_i 1/r_i$, where the r_i are the resistances for all different types of channels in the horizontal cell membrane. These can be simple Ohmic leakage channels as well as postsynaptic channels driven by transmitter release from photoreceptors or voltage-gated channels. In the steady state ($\tau \partial V/\partial t = 0$), while the whole retina is illuminated with constant light intensity ($\lambda^2 \Delta V = 0$), the membrane voltage V equals the full-field potential $E = r_m \sum_i E_i/r_i$, with E_i the corresponding reversal potentials over r_i. The time constant of the sheet $\tau = c_m r_m$ depends on the membrane capacitance c_m, which is also given per sheet area. The spatial properties of the network are reflected in the length constant $\lambda = \sqrt{g r_m/(R_s + R_e)}$, where R_s is the coupling resistance and R_e is the corresponding resistance for the extracellular medium. The factor g is determined by the geometry of the lattice ($g = 3/2$; 1; and 3/4 for a triangular, quadratic, and hexagonal network, respectively).

A few assumptions are necessary for deriving the plate equation (see Appendix for details), especially for the existence of the continuum limit: (1) The network has to be homogeneous and isotropic. (2) Adjacent cells are coupled by a constant sheet resistance R_s. (3) The length constant λ has to be greater than the distance between two neighboring cells. Furthermore, the functional dependencies of r_m, τ, λ, and E on the amount of transmitter released by the photoreceptors and/or the membrane potential V have to be defined.

To analyze the effects of nonlinearities due to feedback mechanisms and/or voltage-gated channels, the experimental results were compared with a linear version of the plate equation. So, the crucial assumption of a linear membrane and simple feedforward input from the photoreceptors to the horizontal cells was made; that is, the membrane resistance and therefore τ, λ, and E directly depend on illumination intensity (Naka & Rushton, 1967).

For a theoretical solution to the model, we considered one-dimensional stimuli such as slits and contrast borders in the steady state where $\tau \partial V/\partial t = 0$. Under these conditions, an exponential voltage decay with a decay constant equal to the length constant λ inside a region of constant light is the basic solution of the stationary plate equation, where the value of λ depends on light intensity. To test this, a contrast border was used in the experiments where one side is completely dark and the other has a defined light intensity. For such an illumination paradigm, the potential is expected to decay in both regions exponentially with length constants λ_0 and λ_+ to the corresponding dark and illuminated full-field potentials E_0 and E_+, respectively:

$$V(x, t = \infty) = \begin{cases} c_+ e^{-x/\lambda_+} + E_+, & x \geq 0 \text{ illuminated} \\ c_0 e^{+x/\lambda_0} + E_0, & x < 0 \text{ dark} \end{cases} \tag{2}$$

with the coefficients

$$c_+ = -\frac{E_+ - E_0}{1 + \lambda_0/\lambda_+}$$

$$c_0 = +\frac{E_+ - E_0}{1 + \lambda_+/\lambda_0}$$

ensuring continuity of voltage and its spatial derivative at location $x = 0$. This is theoretically valid for an infinitely extended retina only. However, if the retina spans more than four-times the length constant on both sides of the contrast border, eqn. (2) is still a very good approximation. Using this kind of stimulus, qualitative and quantitative effects of feedback mechanisms or membrane nonlinearities on voltage spread in the steady state can be detected by deviations from the expectations of the linear plate equation.

In addition, the temporal dynamics of the responses and length constants were computed numerically from the linear plate equation. For that purpose the time courses of the three parameters τ, λ, and E are needed. In the linear model, these parameters are determined by the resistance r_p of the postsynaptic channels driven by the photoreceptor's activity. The corresponding reversal potential of these synaptic channels is close to zero, $E_p = 0$ mV (Miyachi & Murakami, 1991; Golard et al., 1992; Miyachi et al., 1994). Then the numerator ϵ of the full-field potential E is constant

https://doi.org/10.1017/S0952523801155161 Published online by Cambridge University Press

and E depends as well as τ and λ only on the total membrane resistance r_m:

$$E = r_m\left(E_p/r_p + \sum_i E_i/r_i\right) = r_m \sum_i E_i\, r_i := r_m \epsilon.$$

This simplification can be achieved also for a nonzero synaptic reversal potential, if E_p instead of the extracellular potential is used as the reference potential. By means of this relation, the values of τ, λ, and E are connected *via*

$$\tau/\tau_0 = \lambda^2/\lambda_0^2 = E/E_0 = r_m/r_{m,0}, \tag{3}$$

where τ_0, λ_0, E_0, and $r_{m,0}$ are the values of the parameters in the dark. Using this relation the time course of the full-field potential $E(t)$ can be calculated from experimentally measured full-field responses, where the diffusion term in the plate equation vanishes:

$$E(t) = \frac{V(t)}{1 - \dfrac{\tau_0}{E_0}\dfrac{\partial V(t)}{\partial t}}. \tag{4}$$

Due to eq. (3), $E(t)$ completely determines the response $V(x,t)$ of the linear plate eqn. [eqn. (1)], which was computed by Euler backward integration from

$$\tau_0 \frac{E(x,t)}{E_0}\frac{\partial V}{\partial t} = \lambda_0^2 \frac{E(x,t)}{E_0}\Delta V - V + E(x,t), \tag{5}$$

where eqn. (3) is used again. In the dark region ($x < 0$), $E(x,t)$ is set to the dark full-field potential E_0, and in the illuminated region $E(x,t)$ is set to the time course of the illuminated full-field potential, which is calculated from experimental data using eqn. (4). As for the experimental data, length constants of the potential spread in the model can be obtained by fitting eqn. (2) to the computed response $V(x,t)$. For the dark full-field potential, we used $E_0 = -20$ mV, which was the average dark resting potential from our recordings. The value of λ_0 just scales space and was set to the experimentally obtained steady-state value. For the time constant τ_0, we used three values: 5, 10, and 20 ms.

Preparation

Experiments were carried out on everted eyecup preparations of fresh water turtles *Pseudemys scripta elegans* according to European Communities Council Directive (86/609/EEC). The eyecup was prepared as described previously (Itzhaki & Perlman, 1984; Ammermüller & Kolb, 1995). The eye was hemisected with a razor blade and the anterior part was discarded. After removing the vitreous humor, the posterior eyecup was everted over a balsawood dome and placed in a chamber. A continuous flow of normal turtle saline solution was directed over the preparation (Perlman & Ammermüller, 1994).

Light stimulation

The photostimulation system consisted of two light beams originating from a single light source (100-W halogen). The contrast border was formed in the first (= test) beam by a completely dark field opposite to an illuminated field of 649-nm spectral light which was produced with a narrow-band interference filter. Intensity of the illuminated field could be changed by neutral density filters. Dark and illuminated fields were larger than the retina, respectively. The image of the contrast border was focussed on the retina, perpendicular to the visual streak. Contrast was controlled with a CCD array, and it was assured that no stray light reached the retina. Focus on the retina was controlled through a binocular. Between flashes the contrast border could be moved to new retinal positions with a microdrive. Movement steps ranged from 33 μm to 65 μm on the retina. This resulted also in a size change of the illuminated and dark fields on the retina. Direction of movement was parallel to the visual streak to ensure the symmetry of the recording and stimulation procedure and eliminate regional retinal variations. The second (= control) beam of 621 nm was used to illuminate the entire retina and elicit responses in the dynamic range of the cells. Test and control stimulus duration was 800 ms and 600 ms, respectively, separated by an 800-ms dark period. Electronically operated shutters controlled flash duration and interstimulus intervals. The next stimulus pair with the moved contrast border followed after a 1.2-s dark period. Light intensity was measured with a calibrated photodiode at the location of the retina and is expressed as logarithm of the relative intensity (log. rel. int. = 0 was 3.4 mW/cm^2/s at 649 nm for the test, and 2.1 mW/cm^2/s at 621 nm for the control stimuli).

Data acquisition

Sharp glass microelectrodes filled with 3 M potassium acetate (electrode resistances = 100–300 MΩ) were used for intracellular recordings. Amplified signals were digitized at 2000 Hz and stored on a Macintosh PC (MacLab; ADInstruments, Hastings, UK). All recordings were made from the dorsal retina, opposite to the optic nerve head, with the visual streak as landmark. Only data from L1-type horizontal cells, which correspond morphologically to the electrically coupled syncytium of H1 horizontal cell axon terminals, were included in this analysis (Ammermüller & Kolb; 1996). They were identified following previously established criteria (Fuortes & Simon, 1974; Itzhaki & Perlman, 1984; Perlman et al., 1994).

After identification of an L1-type horizontal cell with light stimuli from the control beam, the contrast border from the test beam was centered on the electrode tip and stimulation with the test/control light flashes started. Fig. 1a shows an example of such an unfiltered response pair.

After every stimulation period the contrast border was moved and the next stimulus pair followed. This was repeated until a total deflection of 1.5–2 mm on each side of the centered position was reached. After one complete scan, inclusive control stimuli at the centered position, the intensity of the illuminated field was changed, and the whole series was repeated. This was done for as many intensities as possible. Each scan consisted of 50–100 responses to the stimulation pair.

Data analysis

Specific software was developed in ANSI-C to simplify data processing, using gnuplot for graphical output. The first pass determined resting potentials, peak amplitudes, and plateau amplitudes of test and control responses (see Fig. 1a). The averaged potential in the 100-ms interval before stimulus onset was taken as the resting potential. It was subtracted from the response data, and a 45-Hz low pass filter was applied yielding the relative response. From these smoothed data, the peak amplitude was determined as

https://doi.org/10.1017/S0952523801155161 Published online by Cambridge University Press

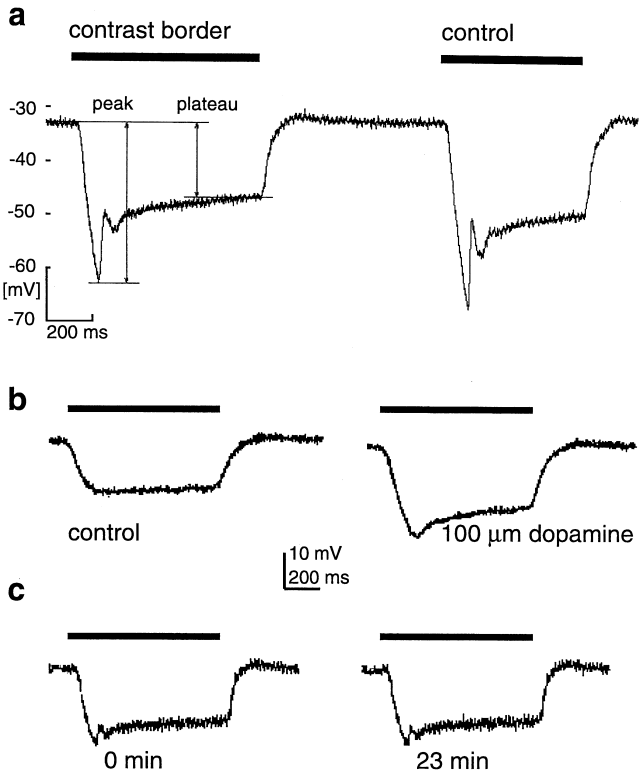

Fig. 1. Experimental protocol and control experiments. (a) Responses of a L1 horizontal cell to a test contrast border (left response) and control (right response) light stimulus. Measuring points for peak and plateau potentials are indicated. Stimulus wavelength was 649 nm for the test, and 621 nm for the control stimulus. Log. rel. int. = −0.5 for both stimuli. (b) Effects of network uncoupling by dopamine on response shape. The response to the centered contrast border became more transient under the influence of 100 μm dopamine, and its amplitude increased. (c) Response shape and amplitude did not significantly change during the course of the length constant measurements. Responses to the contrast border at the beginning of the experiment and after 23 min are shown.

the maximum amplitude during light ON. For the plateau, a straight line was fitted into the unsmoothed data in a 150-ms time window right before the end of the response. Its value at response offset was used as plateau amplitude. As a measure of smoothness, the square root of the mean-squared difference of the unfiltered response to the smoothed one was calculated for the 100-ms interval before stimulus onset. This was divided by the standard deviation of the resting potential. Cells with a smoothness ratio below 0.9 were discarded from analysis since their peak and plateau values were disturbed by too much high-frequency noise.

Peak and plateau amplitudes were corrected for fluctuations in resting potential and response strength. The measured resting potentials of two succeeding responses were linked with a straight line to get a first-order approximation of the resting potential during the response. Differences of this estimated resting potential at peak and plateau to the measured one before response onset were subtracted from the peak and plateau amplitudes, respectively. Mean differences divided by their maximum response amplitudes had to be smaller than 0.12. Changes in response strength were determined by dividing peak and plateau amplitudes of the control responses by the amplitudes of the first control response. Peak and plateau amplitudes of the corresponding test responses were then multiplied by the resulting correction factors. By this way response amplitudes were standardized to the first response, provided the fluctuations were not too large and not too fast. Only data of cells whose correction factors ranged from 0.67 to 1.5, and whose mean difference of the correction factors of two succeeding responses was less than 0.1, were analyzed. In our experience, no stable recording could be obtained from cells with values outside these ranges for a sufficient period of time.

From the corrected relative peak and plateau amplitudes at the various border positions, the length constants were obtained by fitting the steady-state solution of the plate equation [eqn. (2)] to each of the data sets. The central location of the contrast border was ascertained as the turning point of the curve for the peak amplitudes, which was determined using a symmetrical second-order Savitzky-Golay filter (Press et al., 1992). Straight lines were fitted to the last eight data points at the two extreme contrast border positions. To guarantee that the extension of the data to both sides of the contrast border was large enough for the fitting procedure, the slopes of the lines had to be less than 7.5 mV/mm. The illuminated full-field potential E_+ was set to the value of the corresponding fitted line at the last data point, while the dark full-field potential E_o was set to zero. The remaining fit parameters were the length constants for the illuminated (Λ_+) and nonilluminated (Λ_o) parts of the retina. A simplex procedure was used for an initial fit and the Levenberg-Marquard method (Press et al., 1992) was applied for the finishing touches. To use a cell for analysis, at least two complete scans with different intensities inclusive control measurements were required. In the results, the data from 54 complete scans at various intensities obtained from 11 L1-type horizontal cells that fulfilled all the criteria are shown.

Controls

Assuming a constant extracellular resistance R_e, voltage spread in the horizontal cell syncytium is determined by r_m and R_s. To see effects of changes in the sheet resistance R_s three experiments were performed with dopamine superfusion which is known to increase R_s, thereby uncoupling horizontal cells (Dowling, 1991). Under the influence of 100 μM dopamine, light responses to a centered contrast border became more transient and increased in amplitude (Fig. 1b). This is due to increased R_s, reducing lateral voltage spread (Dowling, 1991; Ammermüller et al., 1995). This was never seen in the responses to centered test stimuli in the untreated retinas (Fig. 1c). Even after prolonged experimental time response shape and amplitude remained constant. This demonstrates that intercellular coupling did not change significantly during the experiments.

Geometrical homogeneity of the L1 horizontal cell network was studied in one retina by injecting neurobiotin (Vector Laboratories, Burlingame, CA) into several identified L1 horizontal cells. Electrodes were filled with 4% neurobiotin in 0.4 M KCl, and positive current pulses (+10 to +50 nA; 500-ms duration) were applied at 1 Hz. The retina was fixed for 1 h in 4% paraformaldehyde in 0.1 M phosphate buffer, pH 7.4, washed in buffer, and labeled with the streptavidin–horseradish complex (Jackson Lab., West Grove, PA; 1 : 2 000; containing 0.1% Triton-X) for 12 h. This was followed by a buffer wash and the standard diamino-benzidine/H_2O_2 peroxidase reaction. The neurobiotin labeling showed large networks of coupled H1-axon terminals, which are the morphological correlates of L1 cells (Fig. 2a). Their two-dimensional coverage was analyzed at different retinal locations. Still pictures of selected areas (1.5 mm × 1.1 mm) were

https://doi.org/10.1017/S0952523801155161 Published online by Cambridge University Press

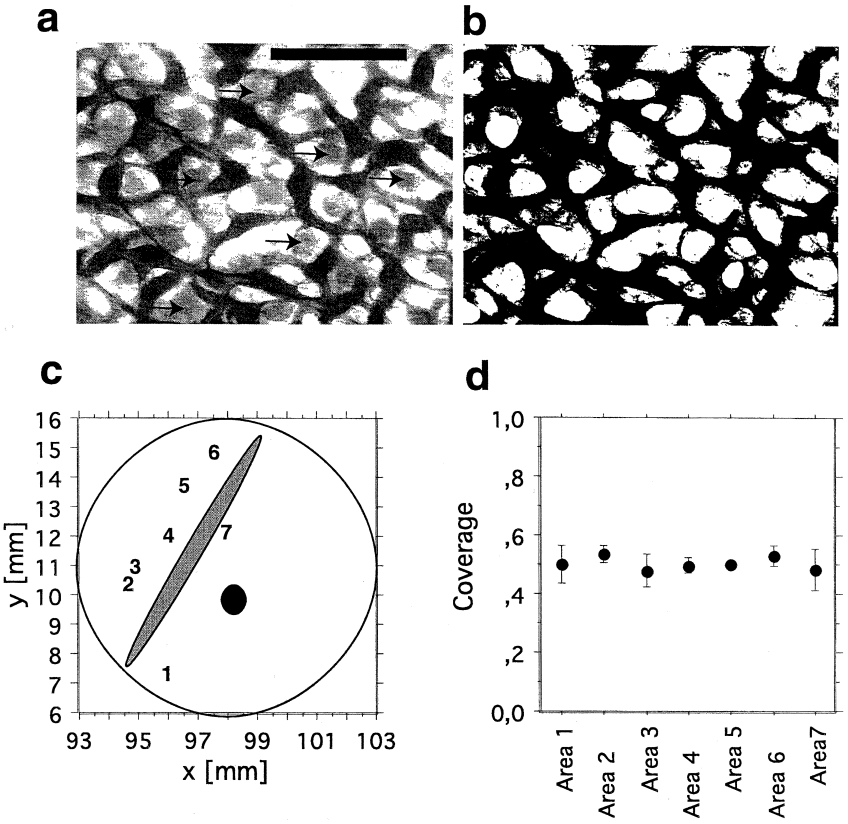

Fig. 2. Relative coverage of H1 axon terminal networks. (a) Video still picture of neurobiotin-labeled axon terminal network obtained after injection of neurobiotin into a L1 horizontal cell. Arrows indicate some of the more weakly labeled H1 somata. Scale = 0.2 mm. (b) One-bit representation of the same picture after image processing and erasing some obvious somata by hand. (c) Schematic representation of the analyzed retinal locations 1–7. At each location, five neighboring areas were measured. Gray ellipse indicates visual streak and black circle optic nerve head. (d) Relative coverage ± SD ($n = 5$) at the seven analyzed locations.

digitized with a color video camera (Kappa Electronics, Göttingen, Germany) at predefined gain and sensitivity values. Neurobiotin injection always resulted in a strong labeling of axon terminals and a weak labeling of H1 cell somata (arrows in Fig. 2a). To measure the homogeneity of the axon terminal network, we processed the images with the program "GraphicConverter" on an Apple PC. After transformation to 16 gray levels, image contrast was enhanced to 100% and gamma to 1.9. This eliminated weakly labeled somata without severely disturbing the axon terminal images. Sometimes somata with stronger labeling had to be erased by hand. A threshold was set and the image was transformed to a black-and-white picture (Fig. 2b). The ratio (number of black pixels)/(number of total pixels) gave us a value for the relative coverage of the axon terminal system. These values are underestimates of the real coverage, since small axon terminal processes out of the focal plane were also eliminated during the procedure. At each indicated retinal location, the coverage of five adjacent areas was measured to determine the variability of this procedure.

Results

Since geometrical homogeneity is one main assumption in the continuum approximation, the relative coverage of the neurobiotin-labeled axon terminal network was measured at different retinal locations, more or less parallel to the visual streak region, where the recordings were made (Fig. 2c). We found no significant change in coverage from center to periphery, over a distance of approximately 8 mm (Fig. 2d). The mean coverage ranged around 0.5 at all locations, which was a good indication that the L1 horizontal cell network is geometrically homogeneous along the axis where the contrast border was moved.

By scanning the retina with the contrast border, voltage distributions as shown in Fig. 3 were obtained. The data points show peak and plateau responses to the contrast border flashed at different retinal positions x (schematically shown for one position in the inset of Fig. 3a). Response amplitudes are expressed relative to the dark full-field potential E_0 which was set to zero as explained in the Methods (Fig. 1a). The electrode position was set to $x = 0$. Positive position values indicate increased area of illumination; negative values indicate decreased area of illumination. The vertical lines and shaded areas illustrate the peak and plateau voltage distribution in the network if a contrast border were flashed centrally at position zero, and one could measure simultaneously at many positions in the dark and illuminated fields of the horizontal cell network. The data points were fitted with the solutions for the contrast border [eqn. (2)] and are shown separately for the peak and plateau potentials (lines in Figs. 3a and 3b). Two length constants Λ_+ and Λ_0 were determined from the fits for the illuminated and nonilluminated regions, respectively. Since it has not been proven at this point that the length constants obtained by these fits are indeed those from the model, which equal $\sqrt{r_m/R_S}$, the measured length constants are denoted with capital lambdas Λ_+ and Λ_o. The fits were always very close to the data points. Fits with a single length constant were also performed (not shown). The quality of the fits was estimated by using $\sqrt{\chi^2/n}$ as a measure of the mean standard deviation of the data points from the fit curve (n = number of data points). These numbers were compared for the single and the two length constants, using the Wilcoxon-Matched-Pairs-Signed-Rank test. The difference be-

https://doi.org/10.1017/S0952523801155161 Published online by Cambridge University Press

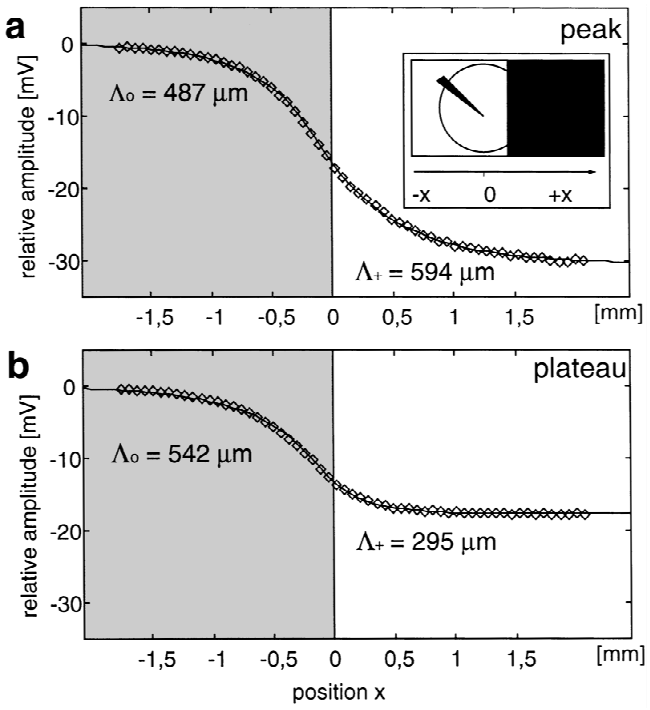

Fig. 3. Dependence of response amplitude on contrast border position for peak (a) and plateau (b) response. The *inset* illustrates how the data points were obtained. The flashed contrast border stimulates the retina (circle) at various positions x. The electrode (arrowhead) records at position $x = 0$. Relative peak and plateau response amplitudes (see Fig. 1a) are plotted against stimulus positions. At the most positive and negative x values, the retina is fully illuminated or not illuminated at all, respectively. Data points (diamonds) were fitted with eqn. (2) in order to yield Λ_o and Λ_+ for both peak and plateau responses (lines). Shading illustrates the equivalent situation if one could record simultaneously at many x positions, and the same contrast border (but with the dark side on the left and the bright side on the right) were flashed at position zero.

tween the fits using one length constant and those using two length constants was highly significant ($P < 0.0001$). The $\sqrt{\chi^2/n}$ values of the fits with Λ_+ and Λ_0 were smaller (0.30 ± 0.03 SEM; $n = 54$) than those of the fits with one length constant (0.34 ± 0.03 SEM; $n = 54$). This shows that two length constants, Λ_+ and Λ_0, are better measures for lateral voltage spread in the horizontal cell syncytium under differentially illuminated regions than a single length constant.

Three important results can be seen in the example of Fig. 3: (1) The voltage spread expressed as Λ_+ and Λ_o was different for the peak and plateau phase of the response indicating temporal dynamics. (2) The length constants were asymmetrical for both the peak and plateau phase of the response, indicating different voltage spread in illuminated and nonilluminated regions. (3) This asymmetry reversed with time from the peak to the plateau phase of the response.

Light-intensity dependence of lateral voltage spread, based on single length-constant calculations, has been shown previously (Byzov & Shura-Bura, 1983; Perlman & Ammermüller, 1994; Reifsnider & Tranchina, 1995; Ammermüller et al., 1996; Kamermans et al., 1996). This effect was also found for both Λ_+ and Λ_o. For one example, this is shown in Fig. 4. The relative peak and plateau responses to full-field illumination were used as a measure of light intensity. For both voltage spread under steady-state conditions (plateau phase) and at the peak response phase, the length constants Λ_+ and Λ_o increased with response amplitude and, therefore, with light intensity. The single length constant for the peak phase was also determined for comparison (crosses in Fig. 4a). Its value ranged between those of Λ_+ and Λ_o and also increased with intensity. Several simple regression models for the function of the increase were tested. Among linear, power, exponential, logarithmic, and reciprocal models, the linear model yielded the best regression coefficients for describing the experimental data points.

The collected data from all experiments are summarized in Table 1. It shows the characteristic values of the linear-regression

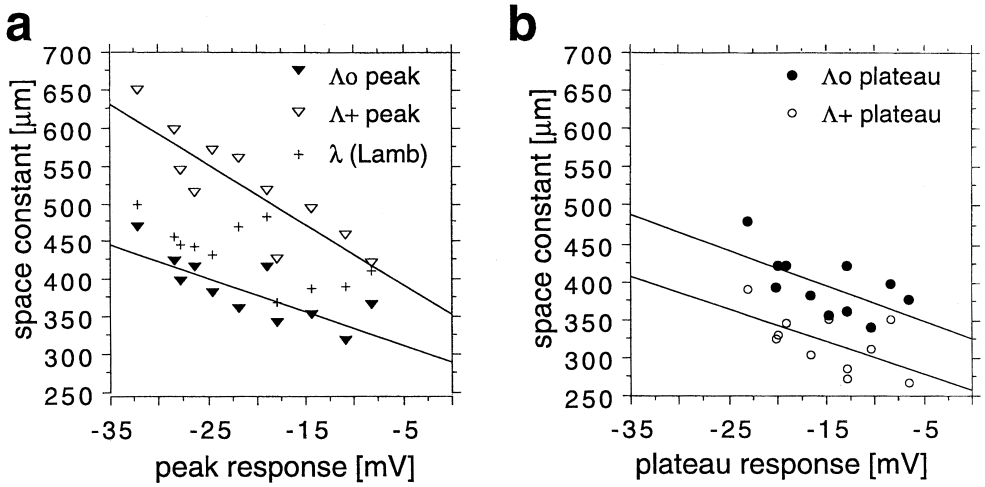

Fig. 4. Dependence of the length constants on light response amplitude for a single L1 horizontal cell. (a) Length constants determined from the peak responses increase with response amplitude in the illuminated (Λ_+; open triangles) and nonilluminated (Λ_o; filled triangles) regions of the retina. The single length constant λ (crosses) is also shown for comparison. (b) Length constants determined from the plateau responses also increase with response amplitude for illuminated (Λ_+ ; open circles) and nonilluminated (Λ_o; filled circles) regions, respectively. Data were best fitted with a linear regression line.

https://doi.org/10.1017/S0952523801155161 Published online by Cambridge University Press

Table 1. *Characteristic values of the linear regression equation* $\Lambda = a + b \cdot |relative\ response|$ *from all data*[a]

	Peak response phase				Plateau response phase			
	Intercept a (μm)	SEM	Slope b (μm/mV)	R^2	Intercept a (μm)	SEM	Slope b (μm/mV)	R^2
Λ_+	389	30.0	5.13	0.303	304	32.2	3.28	0.074
Λ_o	313	25.8	4.69	0.328	399	28.2	4.59	0.231

[a]It describes the light intensity dependence of Λ_o and Λ_+ for the peak and plateau response phases, respectively ($n = 54$).

lines which describe the light-intensity dependence of Λ_+ and Λ_o, both for peak and plateau.

Plotting all cells together resulted in a much larger scatter of the data points than taking data from only a single cell. However, again both length constants, Λ_+ and Λ_o, increased with intensity (slope b in Table 1). Linear regressions were better for the peak than for the plateau phase (R^2 in Table 1). At the peak response phase Λ_+ was on average larger than Λ_o, and in the plateau phase Λ_+ was on average smaller than Λ_o (intercept a in Table 1). This was confirmed by comparing the Λ_+ and Λ_o pairs from each cell with the Wilcoxon-Matched-Pairs-Signed-Rank test. The results were that Λ_+ was significantly ($P < 0.0001$; $n = 54$) larger than Λ_o during the peak phase, and significantly ($P < 0.0001$; $n = 54$) smaller during the plateau phase.

Within the statistical errors, the regression lines were parallel to each other, so both Λ_+ and Λ_o probably showed the same light-intensity dependence. This is illustrated in Fig. 5a where the individual ratios Λ_+/Λ_o are plotted against the response amplitudes. This figure depicts the normalized spatial asymmetry of voltage spread for two points of time, the peak and plateau phase. A ratio of $\Lambda_+/\Lambda_o = 1$ indicates symmetrical voltage spread with respect to the contrast border, and a single length constant would be sufficient to describe it. The measured ratio Λ_+/Λ_o for the peak, however, was on average 1.21 ± 0.02 SEM ($n = 54$), and for the plateau phase 0.76 ± 0.02 SEM ($n = 54$). Testing with the Wilcoxon-One-Sample test yielded a highly significant ($P < 0.0001$) difference to $\Lambda_+/\Lambda_o = 1$ for both cases. We found no statistical indication that the ratios changed with response amplitude. Therefore the asymmetry of voltage spread was light intensity independent, although the absolute Λ_+ and Λ_o values increased with intensity.

The asymmetry in voltage spread was, however, time dependent (see also Figs. 3 and 4). At some point in time between the peak and plateau phase, the ratio Λ_+/Λ_o reversed. To see if these temporal changes were due to changes in both or in one of the length constants, the ratios $\Lambda_{peak}/\Lambda_{plateau}$ were plotted for Λ_+ and Λ_o, respectively, against the peak amplitudes (Fig. 5b). Evidently, Λ_o was nearly the same for both time points. Most of the temporal change in asymmetry was due to changes in Λ_+, which decreased from peak to plateau. At the end of the plateau phase, the mean ratio of $\Lambda_{peak}/\Lambda_{plateau}$ for Λ_+ was 1.53 ± 0.05 SEM ($n = 54$), that is, during the peak phase voltage spread into the illuminated region was 53% larger than during the plateau phase. In contrast, Λ_o did not change very much with time. For Λ_o, the average peak/plateau ratio was 0.90 ± 0.02 SEM ($n = 54$). Voltage spread in the nonilluminated region was 10% larger during the plateau phase compared to the peak phase. Both mean values were significantly different to one ($P < 0.0001$; Wilcoxon-One-Sample test with H_0: $x = 1$). The impression that the peak/plateau ratio of both length constants slightly increased with peak response was not statistically significant.

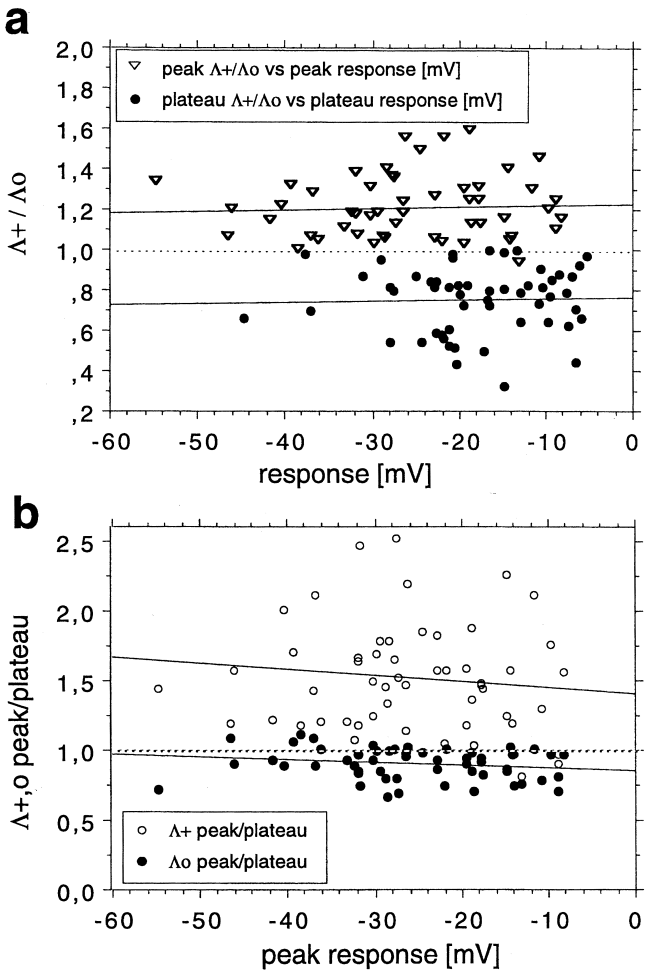

Fig. 5. Dependence of spatial and temporal dynamics of voltage spread on response amplitude and, therefore, on light intensity. (a) The spatial asymmetry (Λ_+/Λ_o) reversed with time from the peak phase to the plateau phase but did not depend on light intensity. (b) The temporal dynamics is shown as the ratio $\Lambda_{peak}/\Lambda_{plateau}$, both for Λ_+ and Λ_o. Λ_o did not change much from peak to plateau, while Λ_+ was larger during peak than during plateau. There was no significant dependence on light intensity.

To obtain a better resolution of the temporal dynamics, 34 scans from six cells were analyzed with more points in time. Fig. 6 shows one example, where the temporal dynamics of voltage spread in illuminated and nonilluminated regions becomes clearer.

https://doi.org/10.1017/S0952523801155161 Published online by Cambridge University Press

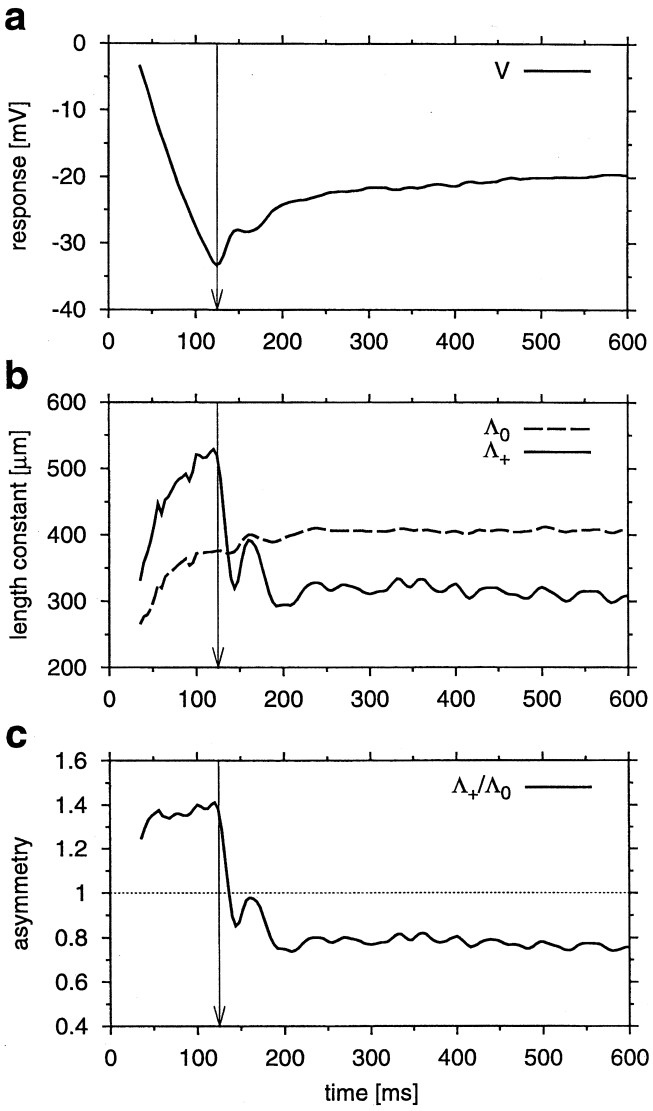

Fig. 6. Temporal dynamics of voltage spread. (a) Light response to the contrast border at position x=1.4mm, which corresponds to a full-field illumination condition. Time zero indicates light onset. Stimulus duration was 800 ms. (b) Temporal dynamics of the two length constants for the illuminated region (Λ_+ solid line) and the nonilluminated region (Λ_o dashed line) of the retina during light on. (c) Time course of asymmetry, expressed as the Λ_+/Λ_o ratio, followed the dynamics of Λ_+. Arrows indicate time of peak response from (a).

This example was chosen because its average ratios of Λ_+/Λ_o and $\Lambda_{peak}/\Lambda_{plateau}$ were similar to the mean values of these ratios in Fig. 5 (Λ_+/Λ_o at peak = 1.39; Λ_+/Λ_o at plateau = 0.76; $\Lambda_{peak}/\Lambda_{plateau}$ = 1.67 under illumination; and $\Lambda_{peak}/\Lambda_{plateau}$ = 0.94 in dark).

In Fig. 6a, the voltage response during illumination with the contrast border is shown. The peak of the response was reached after 125 ms and steady state approximately after 600 ms . Interestingly, the maximum value of Λ_+ preceded the peak response voltage, which is indicated by the arrows in Fig. 6. Immediately after its peak, Λ_+ dropped below Λ_o and both length constants approached a steady-state value. The temporal dynamics of asymmetry is shown in Fig. 6c. Again, the largest deviation of Λ_+/Λ_o from one, indicating the degree of asymmetry, appeared before the peak response. In this example, it lasted for more than 50 ms. Shortly after peak response, voltage spread in illuminated and nonilluminated regions was symmetrical for a short period of time. Finally, the steady-state condition was approached, where voltage spread was larger in the nonilluminated region than in the illuminated region ($\Lambda_+/\Lambda_o < 1$). The same qualitative results were seen in 26 out of the 34 scans. In all the remaining eight cases, Λ_+ at the peak was larger than Λ_o, however, the ratio did not completely reverse during the plateau phase.

To understand where the nonlinear mechanisms come into play, we computed the length constants from the voltage response using the linear plate equation and compared them with the observed time courses (Fig. 7). The time course of the input $E(t)$ was calculated from the experimentally measured dark and illuminated full-field responses as described in the Methods section, using three different values for the membrane time constant at rest (τ_0 = 5, 10, and 20 ms; Fig. 7a). By this way, it was possible to directly compare the results from the linear model with the experimental data for each individual cell and light intensity.

$E(t)$ was always larger than $V(t)$ at the transient response phases, because it has to charge the membrane. The simulated time course of the length constant in the dark, Λ_0, is close to the experimental data (Fig. 7b). There is a tendency for the simulated length constant to approach steady state faster, especially for smaller values of τ_0. For the length constant in the illuminated region, Λ_+, the situation is strikingly different (Fig. 7c). During the first part of the horizontal cell response $V(t)$, before it reaches its peak value, the time courses are quite similar. While at peak time the measured length constant Λ_+ rapidly falls below Λ_0, the simulated ones still increase before they slowly decrease to a steady-state value which is, as expected, well above Λ_0. This peak in the time course of the length constant obtained from the linear model is due to the very transient input $E(t)$, which is needed to produce the transient in the full-field response $V(t)$ (see Fig. 7a). Note that the peak in Λ_+ from the linear model is higher and occurs always later than in the experimental data. This peak is less pronounced for larger time constants τ_0 and for less transient voltage responses of the cells. Due to this peak, there exists also some temporal dynamics of asymmetry (Λ_+/Λ_o) in the linear model (Fig. 7d). Asymmetry, however, never reverses from peak to plateau as it was the case in the experimental data.

Discussion

The plate equation

The plate equation [eqn. (1)] for the membrane potential of the horizontal cell syncytium is an ordinary current balance equation for the membrane capacitance and ion currents, extended by a diffusion term $\lambda^2\Delta V$ for lateral current spread through gap junctions. The basic form of the plate equation is not restricted to a linear membrane. All properties of the membrane channels, which may depend locally on the membrane potential of the horizontal cell and on the amount of transmitter released from photoreceptors or other cells, can be described by an appropriate definition of the membrane resistance r_m. In this case, additional equations are necessary to describe the dynamics of the channels. It is important to note that the global parameters τ (time constant), λ (length constant) and E (full-field potential) all depend on the membrane resistance r_m. Therefore these parameters are in general *not* constant. This makes the plate equation different from the very similar

https://doi.org/10.1017/S0952523801155161 Published online by Cambridge University Press

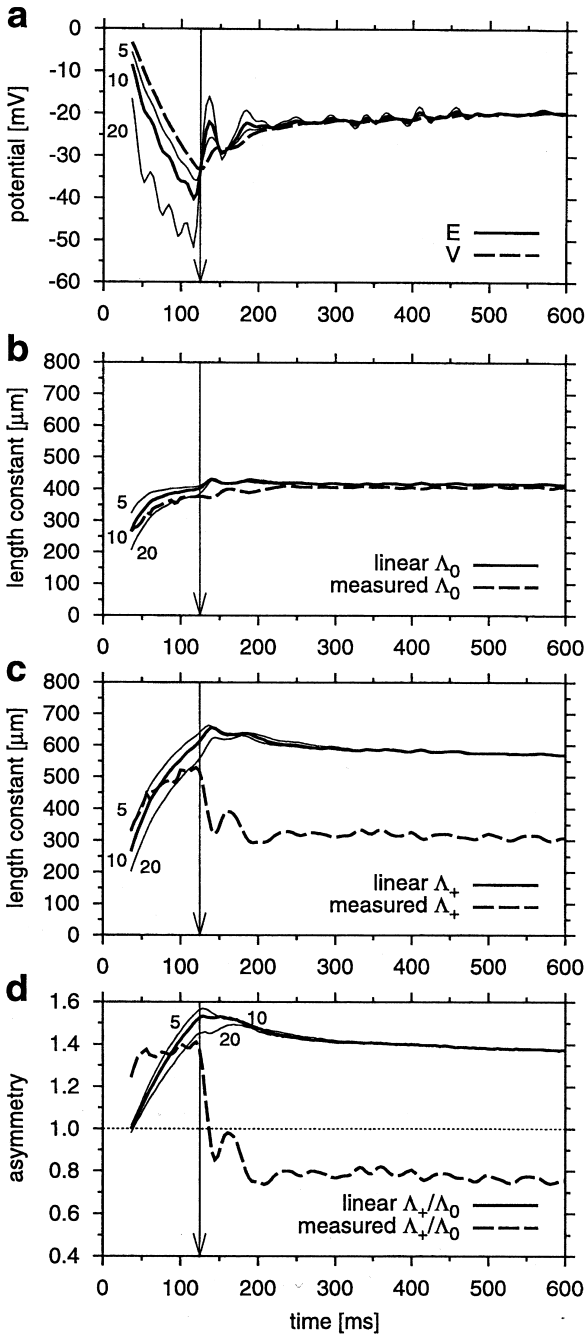

Fig. 7. Comparison of the measured time courses with those calculated from the linear model. (a) Time course of the computed full-field potentials $E(t)$ (solid lines) needed to evoke the measured full-field response $V(t)$ (dashed line) for three different values of τ_0 used for the computation (5, 10, and 20 ms as indicated). (b) Time course of the length constant Λ_o in the nonilluminated part. The computed length constants from the linear model [solid lines, τ_o as in (a)] were very similar to the experimentally obtained one (dashed line). Computed length constants reached steady state a little bit earlier for $\tau_o = 5$ or 10 ms. (c) Time course of Λ_+ in the illuminated part of the retina. At the beginning computed length constants [solid lines, τ_o as in (a)] are similar to the measured one (dashed line), but shortly before the full-field response reached its peak value (indicated by the arrow), the measured length constant decreased and dropped below the values of Λ_o. The computed length constants decreased only slightly and finally stayed at values larger than Λ_o. (d) Asymmetry of voltage spread, expressed as the Λ_+/Λ_o ratio, did not reverse in the linear model, as it was the case in the experiment.

cable equation used for modeling passive cables (Rall, 1977). While in the cable equation, all three parameters are constant and the cable is stimulated by point-like current injections, the syncytium is stimulated continuously in space *via* changes of all three parameters.

The geometric details of the horizontal cell network are reflected by the value of λ *via* the scaling factor g (see Methods and Appendix) and the sheet resistance R_s. Therefore changes in geometry, that is, the network pattern, and changes in R_s result in a different scaling of space. The qualitative behavior of the membrane potential remains unchanged as long as the assumptions for the continuum limit are fulfilled (see below). So, the existence of the continuum limit justifies the use of quadratic or triangular grids for simulation studies (Lamb & Simon, 1976; Winslow & Knapp, 1991; Oshima et al., 1995; Kamermans et al., 1996) as an approximation of the real horizontal cell network. More realistic grids are only needed for a better description of quantitative effects or in conditions where the continuum limit is not valid (Ammermüller et al., 1996; Andreau et al., 2000). It is also sufficient to use one-dimensional grids to study the membrane potential for one-dimensional stimuli such as slits.

The diffusion term

The diffusion term relies on some assumptions: (1) The horizontal cell network has to be homogeneous and isotropic. (2) Adjacent cells are coupled by a constant sheet resistance R_s. (3) The length constant λ has to be greater than the distance between two neighboring cells. This is the essential restriction, which justifies the use of the continuum limit. Our experimental results confirmed indeed these assumptions:

1. The area density was homogeneous across the analyzed area of the retina (Fig. 2d). The control experiments with dopamine superfusion showed that the global coupling of the horizontal cell syncytium under the same stimulus conditions did not change with time. There still exists the possibility that the bipartite field produced heterogeneous coupling of the horizontal cell syncytium by closing gap junctions in the illuminated region of the retina. This would produce a decrease of Λ_+. Several modulators like dopamine (Piccolino et al., 1984), nitric oxide (Pottek et al., 1997), retinoic acid (Weiler et al., 1999), calcium (DeVries & Schwartz, 1992), or pH (Hampson et al., 1994) are known to influence horizontal cell coupling. Many arguments speak against a role of dopamine in heterogeneous uncoupling under our experimental conditions. In the turtle retina, only wide-field A28 amacrine cells with dendritic diameters in the range of 0.5 mm contain dopamine (Kolb et al., 1987, 1997). It is released in the inner plexiform layer (IPL) and has to reach the outer plexiform layer (OPL) by diffusion (Witkovsky et al., 1987, 1993). Therefore, it is very unlikely that the putative action of dopamine is restricted to the illuminated part. Global uncoupling of the syncytium, however, would have been detected in the control experiments. A second argument arises from the fast onset of the change in Λ_+, which occurs around 120 ms after light ON (Fig. 6b). The A28 amacrine cell response has a latency of around 50–100 ms (Kolb et al., 1997), leaving only 20–70 ms for dopamine release, diffusion from the IPL to the OPL, and for triggering the entire dopamine/cAMP cascade. This time seems much too short for us. It takes several tens of seconds

https://doi.org/10.1017/S0952523801155161 Published online by Cambridge University Press

during constant superfusion with dopamine until an initial effect can be observed. The full effect needs several minutes to develop (Piccolino et al., 1984; Ammermüller et al., 1995). Much less is known about the cellular origins and the mechanisms of release and action of the other possible modulators. A final argument, however, speaks against any heterogeneity in coupling between illuminated and nonilluminated parts of the horizontal cell syncytium, that is, a modulation of the sheet resistance due to illumination intensity. A strong dependence of asymmetry (the Λ_+/Λ_o ratio) on peak or plateau potential would be expected, since the horizontal cell response reflects illumination intensity. This was clearly not the case (Fig. 5a). This also excludes the possibility that differences in horizontal cell potential between illuminated and nonilluminated regions *per se* produced heterogeneity in coupling. Since there is no indication for nonisotropy of gap junction density or conductance of the L1 horizontal cell syncytium, we assume that the conditions of homogeneity and isotropy are fulfilled under our experimental conditions.

2. Kaneko (1971) showed that the sheet resistance is indeed Ohmic, that is, the sheet currents are linear. As long as the transjunctional voltage is less than ± 20 mV, gap junctions form Ohmic resistances (DeVries & Schwartz, 1992; Bruzzone et al., 1996). The physiological range of transjunctional voltage of neighboring horizontal cells was estimated to be less than 20 mV in the worst case. As shown in the Appendix [eqn. (A9)], additional currents for hypothetical capacities of the gap junctions can be neglected. Therefore, the sheet resistance is indeed constant.

3. As can be seen from Figs. 2a and 3a, the distance a between two adjacent axon terminals is less than 100 μm and thus smaller than the Λ values which range between 250 and 700 μm, yielding Λ/a ratios larger than 1 (see also Piccolino et al., 1984). Therefore, the condition for the continuum limit is given (see Fig. A-2 in Appendix).

Taking all arguments together, we conclude that under our experimental conditions the continuum limit is valid. There is no reason to question the general plate equation. All effects of voltage spread dynamics that differ from expectations of the linear model have to be attributed to nonlinearities in the membrane current I_m.

Length constants

The reported dependence of lambda on illumination intensity suggested that voltage spread in the horizontal cell network is different in illuminated and nonilluminated parts of the retina (Lamb, 1976; Byzov & Shura-Bura, 1983; Perlman & Ammermüller, 1994; Reifsnider & Tranchina, 1995; Ammermüller et al., 1996; Kamermans et al., 1996). In the most simple scenario, illumination leads to decreased transmitter release from the photoreceptors, thereby closing ionotropic glutamate receptor channels of the horizontal cells (Lasater & Dowling, 1982; Slaughter & Miller, 1983; Miyachi, 1988; Zhou et al., 1993; Krizaj et al., 1994) and increasing the membrane resistance r_m in the illuminated area. Based on a linear continuum model, which takes such changes of r_m into account, one would expect for the steady state that (1) two different length constants exist for illuminated and nonilluminated parts of a retina stimulated with a contrast border; (2) λ_+, the length constant in the illuminated part, increases with increasing intensity; (3) λ_o, the length constant in the nonilluminated part, is independent of intensity; (4) λ_+ is larger than λ_o. These expectations as proposed by Naka and Rushton (1967) have never been validated experimentally, since Lamb (1976) introduced the simplification $\lambda_+ = \lambda_o$ for dim illumination (which was inspired by cable theory, where current like stimuli only attribute to E and not to r_m).

Here we found that the description of voltage spread under a contrast border is indeed more accurately described by exponential functions with two length constants Λ_+ and Λ_o than with a single length constant. Although the peak phase of the response is not covered by the steady-state solutions from the linear model, the fits proved to be as good as those in the plateau phase. So, Λ_+ and Λ_o can be used to describe temporal dynamics of voltage spread under differently illuminated areas phenomenologically. Both Λ_+ and Λ_o increased with light intensity in peak and plateau as shown for the single length constant (Lamb, 1976; Perlman & Ammermüller, 1994; Ammermüller et al., 1995). In addition, voltage spread was asymmetrical with respect to the contrast border. The asymmetry was not intensity dependent, but showed strong temporal dynamics and reversed with time. This temporal change is mainly carried by Λ_+, that is, in the illuminated part of the retina.

Altogether, the last two expectations from the steady-state solution of the linear model were contradicted by the experiments. In the peak response phase, however, where the steady-state condition is not strictly fulfilled, the last prediction that Λ_+ is larger than Λ_o was also supported. This partial failure of the linear plate equation makes it impossible to identify the measured length constants Λ with those from the model λ. So, direct conclusions about the membrane resistance r_m and the sheet resistance R_s *via* the well-known formula $\lambda = \sqrt{r_m/R_S}$ are not valid.

Dynamics of length constants

In Fig. 7 the input for the linear model, $E(t)$, was calculated to result exactly in the measured full-field response. If only synaptic conductances are changed, then $E(t)$ is directly proportional to the total membrane resistance r_m [eqn. (3)]. Therefore, $E(t)$ resembles its time course, including effects of obviously existing nonlinearities. For the linear model, this full-field input is assumed to be the same for all *illuminated* cells. However, in real horizontal cells the feedback strength and/or the state of voltage-gated channels are determined by the illumination strength *and* the membrane potential. Due to the spatially different potential their effective input varies across the contrast border. Neglecting these effects at the moment, then as a linear network $E(t)$ is exactly what the horizontal cells in the illuminated region should get from the photoreceptors. Isolated cones show transient light responses, even without a feedback signal from horizontal cells (Nakatani & Yau, 1988; Matthews et al., 1988, 1990; Schnapf et al., 1990). So, the required transient time course of $E(t)$ is plausible. It is this transient behavior of the input $E(t)$ which is the reason for a peak in Λ_+. Even with this transient input, however, the linear model failed to reproduce three features of the experimental data. First, the large decrease of Λ_+ after an initial peak, leading to the temporal reversal of asymmetry, is in contrast to the linear model. Second, the time course of Λ_+ reaches its peak before the membrane potential, whereas in the simulation it lags behind. Third, the linear model cannot explain the intensity dependence of Λ_o. On the other hand, the linear model reproduced the early phase of Λ_+ and the total time course of Λ_o very well (Fig. 7).

https://doi.org/10.1017/S0952523801155161 Published online by Cambridge University Press

Implications of nonlinearities

Since there is no reason to question the diffusion term of the plate equation, the differences result from the assumption of linearity used for modeling the membrane current I_m. To explain the experimental findings, voltage-dependent nonlinearities must exist. These could be mediated directly by voltage-gated channels, especially potassium and calcium channels in the horizontal cell membrane (Byzov & Trifonov, 1981; Winslow & Knapp, 1991; Golard et al., 1992; Akopian et al., 1997). On the other hand, strong indications exist for an indirect negative feedback pathway *via* the photoreceptors. The mechanisms and parameters of feedback are still under discussion (Wu, 1992; Burkhardt, 1993; Piccolino, 1995; Verweij et al., 1996*a*; Kamermans & Spekreijse, 1999; Kamermans et al., 2001).

Due to such nonlinearities, the spatial voltage distribution in the horizontal cell syncytium leads to a spatially nonuniform membrane resistance, especially in the neighborhood of the contrast border. In Fig. 8, the consequences of this effect are illustrated schematically for the steady-state condition using a simple model. We have to emphasize that this illustration is not aimed to reproduce or explain our findings, but to show some basic principles. The quantitative results will depend on the exact reversal potentials and the transfer functions and/or voltage dependence of the nonlinearities. Using appropriate parameters, nearly any results can be obtained. In this illustration, we assumed a simple feedback which reduced the membrane resistance r_m by an amount proportional to the horizontal membrane potential $V(x)$ relative to its resting potential E_0 (a voltage-gated channel with its reversal potential above resting potential that opens at more negative potentials would, e.g., have the same qualitative effects). The results are that the length constants, as well as the full-field potential E (and the membrane time constant, which is not shown for simplicity), are no longer constant *in space*. All of them also depend on location relative to the contrast border *via* the membrane potential. For example, the membrane length constant depends on illumination intensity *I and* on location *x via* the membrane potential V: $\lambda(I, V(x)) = \sqrt{r_m(I, V(x))/R_S}$. Only far away from the illumination border, where the membrane potential reaches its full-field values, did the three parameters also reach their full-field values.

The interplay of $\lambda(I, V)$ and $E(I, V)$ with the membrane potential V shapes the spatial distribution of the membrane potential delayed by the membrane time constant τ. From that two length constants Λ_0 and Λ_+ can be measured which do neither equal the membrane length constant λ nor allow simple conclusions about the membrane resistance. In the example of Fig. 8, the length constants Λ_0 and Λ_+ are, for example, smaller than any of the corresponding theoretical length constants, since the spatial dependence of the full-field potential additionally shortens voltage decay. Experimentally measured length constants Λ_+ and Λ_o are, however, still a measure of the effective voltage spread, that is, the size of the horizontal cell's receptive field. They are the appropriate parameters for discussing the functional implications of the dynamics of receptive fields in horizontal cells. The decrease of the length constant in the illuminated region after onset of nonlinearities sharpens, for example, the response of the horizontal cells and induces a larger hyperpolarization at the contrast border.

One might argue that as long as the evoked potentials are very small the effects of the nonlinearities are negligible. However, as Fig. 5a shows even for plateau responses of about 5 mV below rest, Λ_+ is clearly below Λ_o, rejecting such an assumption. In addition,

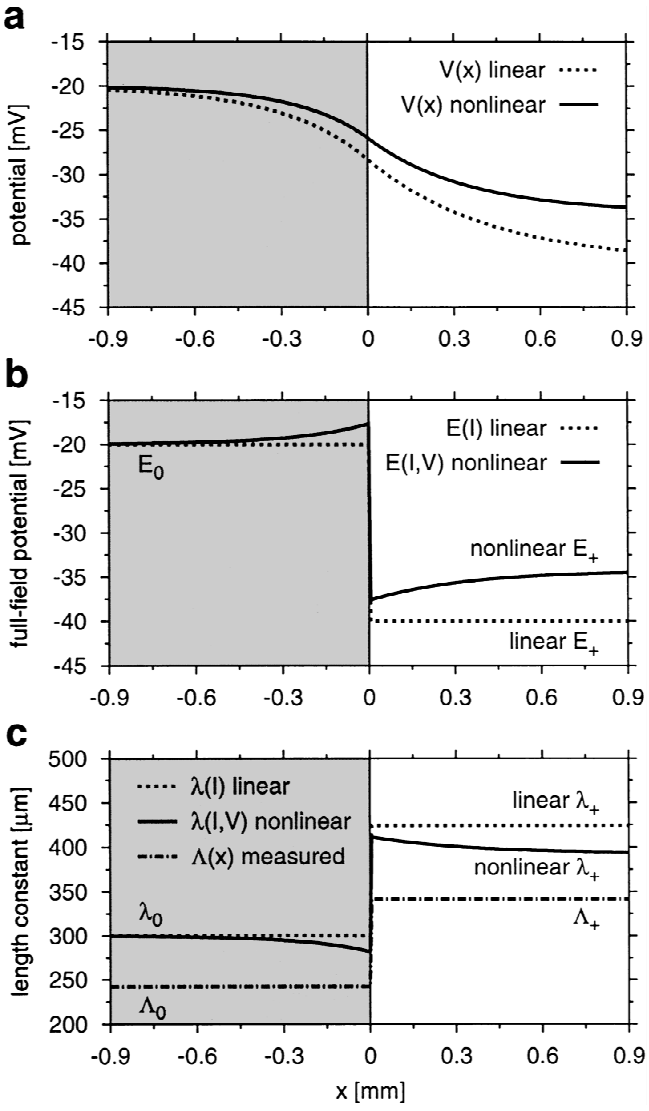

Fig. 8. Demonstration of spatially nonconstant membrane length constants and full-field potentials in the steady state resulting from some nonlinearities in the plate equation. In this simulation, a simple feedback reducing the mebrane resistance r_m by an amount proportional to the horizontal membrane potential V relative to its resting potential E_0 was assumed. The retina was illuminated in the right half ($x > 0$) and remained dark in the left half ($x < 0$). (a) The resulting membrane potential distribution for the linear (dashed line) and nonlinear plate equation (solid line). (b) Due to the nonlinearity, the full-field potential E is reduced (solid line) compared to the linear model (dashed line), which yields constant values for E_0 and E_+ in the dark and illuminated part, respectively. (c) The membrane length constants of the nonlinear model are reduced compared to the linear case. The resulting measured length constants Λ_o and Λ_+ have completely different values, since the distribution of the full-field potential also influences potential spread.

it is very speculative to make any statement about a decrease or increase of r_m from changes observed in the measured length constants because of the complex interaction of the existing nonlinearities with spatial voltage diffusion. Therefore, length-constant data derived from the potential measurements in the center of spots of light with different diameters have to interpreted very carefully, since they are in no way a direct measure of the membrane

https://doi.org/10.1017/S0952523801155161 Published online by Cambridge University Press

resistance. The same holds for length constants measured from the decay of the membrane potential evoked by thin slits of light. These correspond basically to Λ_o from our experiments.

To relate the measured spatio-temporal dynamics of voltage spread with biophysical parameters like r_m, some critical experiments are needed. By pharmacological treatment the relative contributions of feedback, voltage-dependent conductances, or even a completely new mechanism may be separated. In the case of complete blockage of nonlinearities, the linear model should describe all phenomena. Indeed, the complete description of voltage spread by the linear model can be used as a criterion that all nonlinearities are blocked, and the resulting length constant will describe the linear component of r_m. To fully describe the nonlinear behavior, however, *quantitative* descriptions of the equations relating r_m with intensity and membrane potential $V(x)$ are needed. This includes quantitative values for reversal potentials, transfer functions, and voltage dependencies. Presently, the available data about feedback and/or voltage-dependent conductances contain too many free, unknown parameters. Since nearly any result can be obtained in a nonlinear model by using appropriate parameters, conclusions about precise mechanisms seem too speculative for us at present. One has to be aware that the situation is different with a nonlinear model. With the linear assumption, measured voltage spread can be easily related to r_m since this is the only free parameter left (assuming constant sheet resistance). This is not the case in the nonlinear model. Here r_m is not just a single number but a whole function depending on $V(x)$, which has to be parameterized by several numbers to put forward a realistic analytical equation. On the other hand, the description of voltage spread by such a nonlinear model will greatly enhance understanding of spatio-temporal signal processing in the outer plexiform layer even in the case of complex visual stimuli.

Acknowledgments

This work was supported by grants Am 70/10-1 and SFB 251 to J. Ammermüller and P. Rujan. Travel support by a grant from the German Israeli Foundation (I 186-202.08/94) was supplied to J. Benda.

References

Akopian, A., Krizaj, D. & Witkovsky, P. (1997). Both high- and low voltage-activated calcium currents contribute to the light-evoked responses of luminosity horizontal cells in the *Xenopus* retina. *Brain Research* **762**, 121–130.

Allès, B., Beccaria, M., Del Debbio, L. & Del Real, R. (1995). Continuum limit field theories regularized on a random lattice. *Nuclear Physics B Suppl.* **42**, 737.

Ammermüller, J., Weiler, R. & Perlman, I. (1995). Short-term effects of dopamine on photoreceptors, luminosity- and chromaticity-horizontal cells in the turtle retina. *Visual Neuroscience* **12**, 403–412.

Ammermüller, J.A. & Kolb, H. (1995). The organization of the turtle inner retina. I. ON- and OFF-center pathways. *Journal of Comparative Neurology* **358**, 1–34.

Ammermüller, J. & Kolb, H. (1996). Functional architecture of the turtle retina. *Progress in Retinal and Eye Research* **15**, 393–433.

Ammermüller, J., Möckel, W., Perlman, I. & Röhrenbeck, J. (1996). Effects of horizontal cell network architecture on signal spread in the turtle outer retina. Experiments and simulations. *Vision Research* **36**, 4089–4103.

Andreau, E., Fernandez, E., Louis, E., Ortega, G. & Sanchez-Andres, J.V. (2000). Role of architecture in determining passive electrical properties in gap junction-connected cells. *Pflügers Archiv—European Journal of Physiology* **439**, 789–797.

Bimonte, G., Ercolessi, E., Landi, G., Lizzi, F., Sparano, G. & Teotino-Sobrinho, P. (1996). Lattices and their continuum limits. *Journal of Geometry and Physics* **20**, 318–328.

Boroviagin, W.L. (1966). A submicroscopic morphology and the structural interconnections of receptors and horizontal cells in the retina of some lower vertebrates. *Biophysica* **11**, 810–817.

Bruzzone, R., White, T.W. & Paul, D.L. (1996). Connections with connexins: The molecular basis of direct intercellular signalling. *European Journal of Biochemistry* **238**, 1–27.

Burkhardt, D.A. (1993). Synaptic feedback, depolarization, and color opponency in cone photoreceptors. *Visual Neuroscience* **10**, 981–989.

Byzov, A.L. (1975). Interaction between horizontal cells of the turtle retina. *Neurophysiology* **7**, 279–286.

Byzov, A.L. & Trifonov, Y.A. (1981). Ionic mechanisms underlying the nonlinearity of horizontal cell membranes. *Vision Research* **21**, 1573–1578.

Byzov, A.L. & Shura-Bura, T.M. (1983). Spread of potentials along the network of horizontal cells in the retina of the turtle. *Vision Research* **23**, 389–397.

Christ, N.H., Friedberg, R. & Lee, T.D. (1982). Random lattice field theory: General formulation. *Nuclear Physics* **B202**, 89–125.

DeVries, S.H. & Schwartz, E.A. (1989). Modulation of an electrical synapse between solitary pairs of catfish horizontal cells by dopamine and second messengers. *Journal of Physiology* (London) **414**, 351–375.

DeVries, S.H. & Schwartz, E.A. (1992). Hemi-gap-junction channels in solitary horizontal cells of the catfish retina. *Journal of Physiology* (London) **445**, 201–230.

Dowling, J.E. (1991). Retinal neuromodulation: The role of dopamine. *Visual Neuroscience* **7**, 87–97.

Fuortes, M.G.F. & Simon, E.J. (1974). Interactions leading to horizontal cell responses in the turtle retina. *Journal of Physiology* **240**, 177–198.

Gerschenfeld, H.M., Neyton, J., Piccolino, M. & Witkovsky, P. (1982). L-horizontal cells of the turtle: Network organization and coupling modulation. *Biomedical Research* (Suppl.) **3**, 21–32.

Golard, A., Witkovsky, P. & Tranchina, D. (1992). Membrane currents of horizontal cells isolated from turtle retina. *Journal of Neurophysiology* **68**, 351–361.

Hampson, E.C.G.M., Weiler, R. & Vaney, D.I. (1994). pH-Gated dopaminergic modulation of horizontal cell gap junctions in mammalian retina. *Proceedings of the Royal Society B* (London) **255**, 67–72.

Itzhaki, A. & Perlman, I. (1984). Light adaptation in luminosity horizontal cells in the turtle retina: Role of cellular coupling. *Vision Research* **24**, 1119–1126.

Kamermans, M. & Spekreijse, H. (1999). The feedback pathway from horizontal cells to cones. A mini review with look ahead. *Vision Research* **39**, 2449–2468.

Kamermans, M., Haak, J., Habraken, J.B.A. & Spekreijse, H. (1996). The size of the horizontal receptive fields adapts to the stimulus in the light adapted goldfish retina. *Vision Research* **24**, 4105–4120.

Kamermans, M., Fahrenfort, I., Schultz, K., Janssen-Bienhold, U. & Weiler, R. (2001). Hemichannel mediated inhibition in the outer retina. *Science* **292**, 1178–1180.

Kaneko, A. (1971). Electrical connections between horizontal cells in the dogfish retina. *Journal of Physiology* **213**, 95–105.

Kolb, H., Cline, C., Wang, H.H. & Brecha, N. (1987). Distribution and morphology of dopaminergic amacrine cells in the retina of the *turtle (Pseudemys scripta elegans). Journal of Neurocytology* **16**, 577–588.

Kolb, H., Netzer, E. & Ammermüller, J. (1997). Neural circuitry and light responses of the dopamine amacrine cell of the turtle retina. *Molecular Vision* **3**, 6. ⟨http://www.emory.edu/molvis/v3/kolb⟩

Krizaj, D., Akopian, A. & Witkovsky, P. (1994). The effects of L-glutamate, AMPA, quisqualate, and kainate on retinal horizontal cells depend on adaptational state: Implications for rod–cone interactions. *Journal of Neuroscience* **14**, 5661–5671.

Lamb, T.D. (1976). Spatial properties of horizontal cell responses in the turtle retina. *Journal of Physiology* **263**, 239–255.

Lamb, T.D. & Simon, E.J. (1976). The relation between intercellular coupling and electrical noise in turtle photoreceptors. *Journal of Physiology* **263**, 257–286.

Lankheet, M.J.M., Frens, M.A. & van de Grind, W.A. (1990). Spatial properties of horizontal cell responses in the cat retina. *Vision Research* **30**, 1257–1275.

Lankheet, M.J.M., Przybyszewski, A.W. & van de Grind, W.A. (1993). The lateral spread of light adaptation in cat horizontal cell responses. *Vision Research* **33**, 1173–1184.

Lasater, E.M. & Dowling, J.E. (1982). Carp horizontal cells in culture respond selectively to l-glutamate and ist agonists. *Proceedings of the National Academy of Sciences of the U.S.A.* **79**, 936–940.

Mangel, S.C. (1991). Analysis of the horizontal cell contribution to the receptive field surround of ganglion cells in the rabbit retina. *Journal of Physiology* **44**, 211–234.

Marmarelis, P.Z. & Naka, K.-I. (1972). Spatial distribution of potential in a flat cell. Application to the catfish horizontal cell layers. *Biophysical Journal* **12**, 1515–1532.

Matthews, H.R., Murphy, R.L.W., Fain, G.L. & Lamb, T.D. (1988). Photoreceptor light adaptation is mediated by cytoplasmatic calcium concentration. *Nature* **334**, 67–69.

Matthews, H.R., Fain, G.L., Murphy, R.L.W. & Lamb, T.D. (1990). Light adaptation in cone photoreceptors of the salamander: A role for cytoplasmatic calcium. *Journal of Physiology* **420**, 447–469.

Miyachi, E.-I. (1988). Different appearance of actions of excitatory amino acids on turtle horizontal cells in different preparations; eyecup and isolated retina. *Neuroscience Research* (Suppl.) **8**, S211–S215.

Miyachi, E.-I. & Murakami, M. (1991). Synaptic inputs to turtle horizontal cells analyzed after blocking gap junctions by intracellular injection of cyclic nucleotides. *Vision Research* **31**, 631–635.

Miyachi, E.-I., Kato, C. & Nakaki, T. (1994). Arachidonic acid blocks gap junctions between retinal horizontal cells. *NeuroReport* **5**, 485–488.

Naka, K.-I. & Rushton, W.A. (1967). The generation and spread of S-potentials in fish (Cyprinidae). *Journal of Physiology* **193**, 437–461.

Naka, K.-I. & Witkovsky, P. (1972). Dogfish ganglion cell discharge resulting from extrinsic polarization of the horizontal cells. *Journal of Physiology* **223**, 449–460.

Nakatani, K. & Yau, K.-W. (1988). Calcium and light adaptation in retinal rods and cones. *Nature* **334**, 69–71.

Norton, A.L., Spekreijse, H., Wolbarsht, M.L. & Wagner, H.G. (1968). Receptive field organization of the S-potential. *Science* **160**, 1021–1022.

Oshima, S., Yagi, T. & Funahashi, Y. (1995). Computational studies on the interaction between red cone and H1 horizontal cell. *Vision Research* **35**, 149–160.

Owen, W.G. & Hare, W.A. (1989). Signal transfer from photoreceptors to bipolar cells in the retina of the tiger salamander. *Neuroscience Research* (Suppl.) **10**, 77–88.

Perlman, I. & Ammermüller, J. (1994). Receptive-field size of L1 horizontal cells in the turtle retina: Effects of dopamine and background light. *Journal of Neurophysiology* **72**, 2786–2795.

Perlman, I., Itzhaki, A., Malik, S. & Alpern, M. (1994). The action spectra of cone photoreceptors in the turtle (*Mauremys caspica*) retina. *Visual Neuroscience* **11**, 243–252.

Piccolino, M., Neyton, J. & Gerschenfeld, H.M. (1984). Decrease of gap junction permeability induced by dopamine and cyclic adenosine 3′:5′-monophosphate in horizontal cells of turtle retina. *Journal of Neuroscience* **4**, 2477–2488.

Piccolino, M. (1995). The feedback synapse from horizontal cells to cone photoreceptors in the vertebrate retina. *Progress in Retinal and Eye Research* **14**, 141–196.

Pottek, M., Schultz, K. & Weiler, R. (1997). Effects of nitric oxide on the horizontal cell network and dopamine release in the carp retina. *Vision Research* **37**, 1091–1102.

Press, W.H., Teukolsky, S.A., Vetterling, W.T. & Flannery, B.P. (1992). *Numerical Recipes in C*. New York: Cambridge University Press.

Rall, W. (1977). Core conductor theory and cable properties of neurons. In *Handbook of Physiology. Sect. 1, The Nervous System, Vol. 1*, ed. Kandel, E.R., pp. 39–97. Bethesda, Maryland: American Physiological Society.

Raviola, E. (1976). Intracellular junctions in the outer plexiform layer of the retina. *Investigative Ophthalmology and Visual Science* **15**, 881–894.

Reifsnider, E.S. & Tranchina, D. (1995). Background contrast modulates kinetics and lateral spread of responses to superimposed stimuli in outer retina. *Visual Neuroscience* **12**, 1105–1126.

Schnapf, J.L., Nunn, B.J., Meister, M. & Baylor, D.A. (1990). Visual transduction in cones of the monkey *Macaca fascicularis*. *Journal of Physiology* **427**, 681–713.

Slaughter, M.M. & Miller, R.F. (1983). The role of excitatory amino acid transmitters in the mudpuppy retina: An analysis with kainic acid and N-methyl aspartate. *Journal of Neuroscience* **3**, 1701–1711.

Thibos, L.N. & Werblin, F.S. (1978). The response properties of the steady antagonistic surround in the mudpuppy retina. *Journal of Physiology* **278**, 79–99.

Tomita, T. (1957). A study of the origin of intraretinal action potential of the cyprinid fish by means of a pencil-type microelectrode. *Japanese Journal of Physiology* **7**, 80–85.

Umino, O. & Ushio, T. (1998). Spatio-temporal receptive fields in carp retinal horizontal cells. *Journal of Physiology* **508**, 223–236.

Verweij, J., Kamermans, M. & Spekreijse, H. (1996*a*). Horizontal cells feed back to cones by shifting the cone calcium-current activation range. *Vision Research* **24**, 3943–3954.

Verweij, J., Kamermans, M., van den Aker, E.C. & Spekreijse, H. (1996*b*). Modulation of horizontal cell receptive fields in the light adapted goldfish retina. *Vision Research* **36**, 3913–3923.

Weiler, R., He, S. & Vaney, D.I. (1999). Retinoic acid modulates gap junction permeability between horizontal cells of the mammalian retina. *European Journal of Neuroscience* **11**, 3346–3350.

Werblin, F.S. (1974). Control of retinal sensitivity. II. Lateral interactions at the outer plexiform layer. *Journal of General Physiology* **63**, 62–87.

Winslow, R.L. & Knapp, A.G. (1991). Dynamic models of the retinal horizontal cell network. *Progress in Biophysics and Molecular Biology* **56**, 107–133.

Witkovsky, P., Alones, V. & Piccolino, M. (1987). Morphological changes induced in turtle retinal neurons by exposure to 6-hydroxydopamine and 5,6-dihydroxytryptamine. *Journal of Neurocytology* **16**, 55–67.

Witkovsky, P., Nicholson, C., Rice, M.E., Bohmaker, K. & Meller, E. (1993). Extracellular dopamine concentration in the retina of the clawed frog, Xenopus laevis. *Proceedings of the National Academy of Sciences of the U.S.A.* **90**, 5667–5671.

Wu, S.M. (1992). Feedback connections and operation of the outer plexiform layer of the retina. *Current Opinion in Neurobiology* **2**, 462–468.

Wu, S.M. (1994). Synaptic transmission in the outer retina. *Annual Review of Physiology* **56**, 141–168.

Yagi, T. & Kaneko, A. (1987). Membrane properties and the signal conduction of the horizontal cell syncytium of the teleost retina. *Neuroscience Research* (Suppl.) **6**, S119–S132.

Zhou, Z.J., Fain, G.L. & Dowling, J.E. (1993). The excitatory and inhibitory amino acid receptors on horizontal cells isolated from the white perch retina. *Journal of Neurophysiology* **70**, 8–19.

Appendix

Derivation of the plate equation

A first step in modeling a horizontal cell network is to represent each cell as the vertex of a lattice. Here the plate equation is derived from regular (quadratic or triangular) lattices. Consider a cell at position k and one of its nearest neighbors $k + 1$ in direction j (see Fig. A-1), coupled by the constant sheet resistances $R_{s_k^j}$ due to the gap junctions. The current I_k^j which flows from cell k towards the neighboring cell is due to the potential difference $V_{k+1}^j - V_k$ between them:

$$I_k^j = -\frac{V_{k+1}^j - V_k}{R_{s_k^j}}. \tag{A1}$$

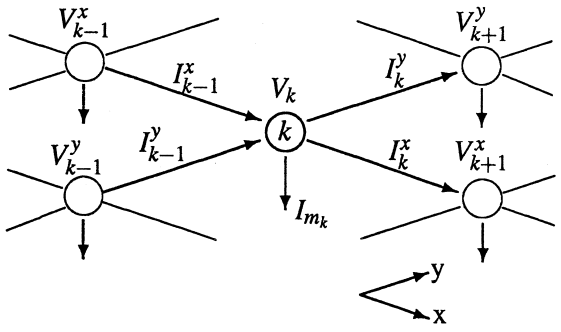

Fig. A-1. A small part of a quadratic lattice with its potentials and currents.

https://doi.org/10.1017/S0952523801155161 Published online by Cambridge University Press

At each node, the sum of currents flowing from all $2Q$ adjacent cells in Q directions j (two for the quadratic and three for the triangular lattice) must match the membrane current I_{m_k} of cell k:

$$I_{m_k} = \sum_{j=1}^{Q} (I_{k-1}^j - I_k^j). \tag{A2}$$

Inserting eqn. (A1) and assuming the sheet resistances to be homogeneous and isotropic, $R_s = R_{s_k^j}$ for all positions k and directions j, this equation can be written as

$$\frac{1}{R_S} \sum_{j=1}^{Q} (V_{k+1}^j - 2V_k + V_{k-1}^j) = I_{m_k}. \tag{A3}$$

Next substitute the membrane current I_{m_k} by the corresponding current density $i_{m_k} = I_{m_k}/A$, where $A = a^2$ is the sheet area of one cell and a is the averaged distance of the cells. We get

$$\frac{1}{R_S} \sum_{j=1}^{Q} \frac{V_{k+1}^j - 2V_k + V_{k-1}^j}{a^2} = i_{m_k}, \tag{A4}$$

which is a sum of second-order differences for all directions j. In the continuum limit $a \to \partial a$, these differences become second-order spatial derivatives, resulting in a simple diffusion-like differential equation:

$$\frac{g}{R_S} \Delta V(\vec{x}) = i_m(\vec{x}), \tag{A5}$$

where $\Delta = \partial^2/\partial x^2 + \partial^2/\partial y^2$ is the two-dimensional Laplace operator, $\vec{x}$ is the location in the horizontal cell layer, and g is a number depending on the geometry of the grid ($g = 1$ for quadratic, $g = 3/2$ for triangular, and $g = 3/4$ for hexagonal lattices). Although this equation is derived for the special case of regular lattices, it is possible to show that the continuum theory can be mapped into any Bravais or even into random lattices (Christ et al., 1982; Allés et al., 1995; Bimonte et al., 1996).

To get an equation for the membrane potential, it is also necessary to specify the membrane current density i_m. It is composed of different ion currents $i_k = (V - E_k)/r_k$ through channels of type k with resistance r_k and corresponding reversal potential E_k. The resistances r_k (Ω m^2) are identical with the resistance per membrane surface multiplied by the relative membrane surface a_m, which is the ratio A_m/A of the total surface of the cell A_m and the sheet area $A = a^2$. The resistances r_k may depend on the activity of the presynaptic photoreceptor or on the potential of the horizontal cell itself. In addition, there is the current due to the membrane capacitance $i_c = c_m \dot{V}$, where c_m (F/m^2) is the time-independent membrane capacity per sheet area. Again, it is identical to the membrane capacity per membrane surface ($c_m' \sim 1$ μF/cm^2) multiplied by the relative membrane surface a_m.

Summing all these membrane currents and inserting them into eqn. (A5), one obtains the plate equation:

$$\tau \dot{V} = \lambda^2 \Delta V - V + E, \tag{A6}$$

where $r_m(\vec{x}, t)$ (Ωm^2) ($1/r_m = \Sigma_k 1/r_k$) is the membrane resistance, $\tau(\vec{x}, t)$ (s) $= c_m r_m$ is the time constant, $\lambda(\vec{x}, t)$ (m) $= \sqrt{g r_m / R_S}$ is the length constant, and $E(\vec{x}, t)$ (V) $= r_m \Sigma_k E_k / r_k$ is the full-field potential. Note that τ, λ, and E depend on retinal position $\vec{x}$ and time t due to the membrane resistance r_m driven by the photoreceptors or the potential of the horizontal cells.

Condition for the continuum limit

The condition for the continuum limit eqn. (A6) to be a good approximation of the discrete cell network was already investigated by Lamb and Simon (1976). On a quadratic grid where $g = 1$, the decay constant for the potential in the steady state is given by

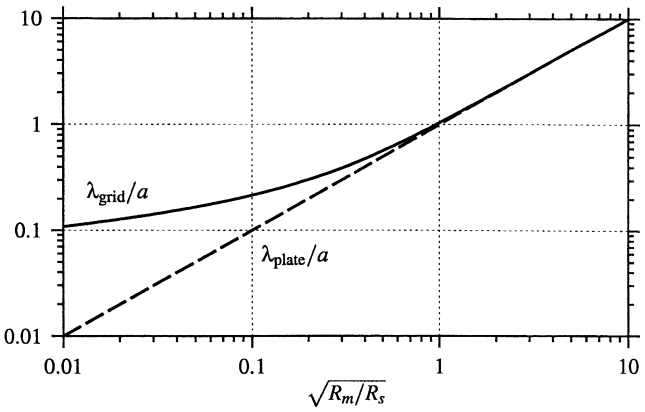

Fig. A-2. The length constants for the exponential decay of the potential on a discrete cell network λ_{grid} and for its continuum approximation λ_{plate}, related to the cell spacing a. Their dependence on the ratio of the membrane resistance R_m and the sheet resistance R_s is shown. If this ratio exceeds one, or if the length constants are greater than the cell distances, the network is approximated very well by the continuum model.

$$\lambda_{\text{grid}} = \frac{a}{\operatorname{arcosh}\left(\frac{R_s}{2R_m} + 1\right)}, \tag{A7}$$

where R_m (Ω) is the total membrane resistance of a single cell, which is related to r_m *via* the sheet area $A = a^2$ by $r_m = R_m A$. On the other hand, the length constant from the plate equation [eqn. (A6)], which also describes the exponential decay in the steady state, is given by

$$\lambda_{\text{plate}} = \sqrt{\frac{r_m}{R_s}} = a\sqrt{\frac{R_m}{R_s}}. \tag{A8}$$

In Fig. A-2, both the grid and the plate-decay constants expressed in the distance a of two adjacent cells are plotted against $\sqrt{R_m/R_s}$. If the length constant of the exponential decay in the steady state is just greater than the spacing of the cells a, the continuum limit gives a very good approximation of the potential in the discrete network.

Capacity of gap junctions

The gap junctions do not only contribute to the sheet resistance R_s but they could also act as little capacitors C_s, coupled in parallel to R_s. To include the effect of such a capacitance, the additional term $\sigma \Delta \dot{V}$ has to be added to the diffusion term in the plate equation [eqn. (A6)], where $\sigma(\vec{x}, t)$ (m^{2}s) $= C_s r_m g$. An estimation of the magnitude of this term as $\sigma(V/\tau\lambda^2)$ in relation to the V term leads to

$$\frac{\sigma \Delta \dot{V}}{V} \approx g \frac{A_g}{A_m} \left(\frac{a}{\lambda}\right)^2, \tag{A9}$$

where the gap junction capacity C_s is estimated by the specific membrane capacitance c_m' times the the total gap junction area of one cell A_g. g—the number depending on the geometry of the grid—is on the order of one. For the continuum limit to be valid, the length constant has to be larger than the distance of adjacent cells: $a/\lambda < 1$. The surface of all gap junctions of a cell is on the order of 1 μm^2, while the surface of a whole cell A_m is on the order of several hundreds μm^2. Taking all this into consideration shows that the gap-junction-capacity term makes less than 1% of the other terms and can hence be neglected. The time derivative it contains is important only for the time-dependent solutions of the plate equation [eqn. (A6)], anyway.

https://doi.org/10.1017/S0952523801155161 Published online by Cambridge University Press